Journal Pre-proof

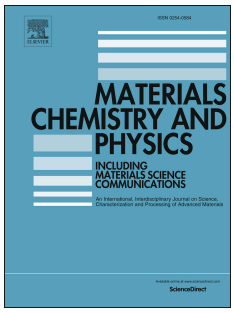

An electrodeposited Au nanoparticle/porous graphene nanoribbon composite for electrochemical detection of alpha-fetoprotein

Lavanya Jothi, Saravana Kumar Jaganathan, Gomathi Nageswaran

PII: S0254-0584(19)31324-0

DOI: https://doi.org/10.1016/j.matchemphys.2019.122514

Reference: MAC 122514

To appear in: *Materials Chemistry and Physics*

Received Date: 9 July 2019

Revised Date: 28 November 2019

Accepted Date: 30 November 2019

Please cite this article as: L. Jothi, S.K. Jaganathan, G. Nageswaran, An electrodeposited Au nanoparticle/porous graphene nanoribbon composite for electrochemical detection of alpha-fetoprotein, *Materials Chemistry and Physics* (2020), doi: https://doi.org/10.1016/j.matchemphys.2019.122514.

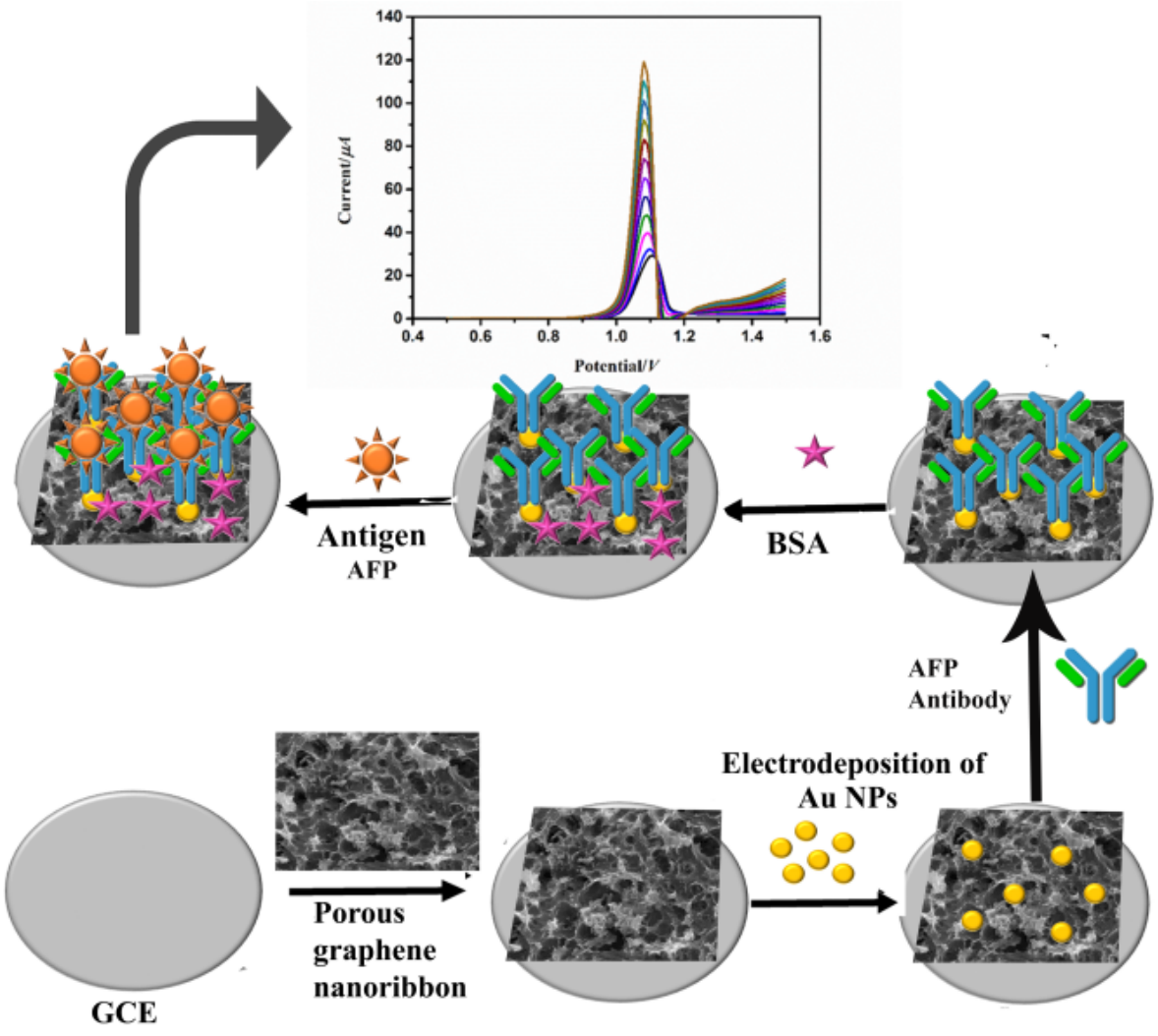
Current/μA
Potential/V
Antigen
AFP
BSA
AFP
Antibody
Electrodeposition of
Au NPs
Porous
graphene
nanoribbon
GCE

An electrodeposited Au nanoparticle/porous graphene nanoribbon composite for electrochemical detection of alpha-fetoprotein

Lavanya Jothi [a], Saravana Kumar Jaganathan[b,c,d], Gomathi Nageswaran[a*]

[a] Department of Chemistry, Indian Institute of Space Science and Technology, Thiruvananthapuram, Kerala, 695547, India

[b] Department for Management of Science and Technology Development, Ton Duc Thang University, Ho Chi Minh City, Vietnam

[c] Faculty of Applied Sciences, Ton Duc Thang University, Ho Chi Minh City, Vietnam

[d] Department of Engineering, Faculty of Science and Engineering, University of Hull, Hull HU6 7RX, UK

Abstract

In this work, a novel label-free electrochemical immunosensor for the detection of alpha-fetoprotein (AFP) is fabricated for early diagnosis and prognostics of liver cancer. A porous graphene nanoribbon (PGNR) was synthesized via chemical reduction method and it was electrodeposited with gold nanoparticles (AuNPs) to obtain AuNPs/PGNR hybrid nanomaterial. Anti-AFP was immobilized onto AuNPs/PGNR/glassy carbon electrode and anti-AFP/AuNPs/PGNR/GCE was further studied to demonstrate its electrocatalytic activity towards AFP antigen. PGNR enhances the electroactive surface area and the electron transfer ability between the electrode and redox probe while the AuNPs deposited on PGNR are used to immobilize biomolecules and to facilitate the electron transport. The superior biosensing performance towards AFP under physiological pH condition is demonstrated by a corresponding decreased peak current in differential pulse voltammetry for a wide linear range (5-60 ng/mL) with a low detection limit of 1 ng/mL. Detection of AFP in serum samples by this label-free electrochemical immunosensor without fouling or significant interference implies that the anti-AFP/AuNPs/PGNR modified GCE has a great application potential for clinical diagnosis of AFP.

Keywords: Porous graphene nanoribbons, gold nanoparticles, alpha fetoprotein, differential pulse voltammetry.

---

*Corresponding author. E-mail: sivakumar.gomathi@gmail.com, gomathi@iist.ac.in (Dr.N.Gomathi) Tel. +91-471-2568552.

1. Introduction

Alpha fetoprotein (AFP), an oncofetal glycoprotein produced by liver, yolksac, and gastrointestinal tract of humans, is considered as a well-known clinical biomarker for hepatocellular carcinoma (HCC) [1,2]. The concentration of AFP for a healthy body is 20 ng mL^{-1}. The increase of AFP above 500 ng mL^{-1} in human serum is an indicator of liver tumor. Therefore, the concentration of AFP can be used as an early indicator for diagnosis and prognostics of HCC and other related diseases like yolk sac cancer, testicular cancer and nasopharyngeal cancer [3–5] . This necessitates the development of a reliable method for sensitive and selective detection of AFP. Among the various detection methods available, such as surface plasmon resonance, quartz crystal microbalance, electrochemical immunosensors, atomic absorption spectrometry, chemiluminescence assay and inductively coupled plasma mass spectrometry, the electrochemical immunosensor has received much attention as the most reliable method for detection of AFP biomarker, owing to its high sensitivity, specificity, rapid detection, cost efficiency, low-temperature requirements and compact instrumentation [6–10]. Furthermore, compared with sandwich-type immunosensor, label-free electrochemical immunosensors have certain advantages, for instance, they could be directly used to diagnose and monitor the level of biomarker and avoid interference from conjugated markers or other endogenous species [11–13] .

Graphene nanoribbons (GNR), possessing excellent physical, chemical, mechanical and biological properties [14,15], have received tremendous scientific attention in a wide range of applications like gas separation, water desalination, energy storage, fuel cells, electrochemical capacitors and drug delivery [16,17]. Owing to its high aspect ratio, tunable electronic properties, abundant edges, and defect sites and high electron transfer rate, it has been considered as a potential electrode material for the fabrication of electrodes in electrochemical sensors. Despite its excellent properties, pristine GNR tends to form irreversible agglomerates or even restack to form graphite through strong $\pi - \pi$ bonds and van der Waal`s interaction. This agglomeration tendency has a deleterious effect on most of its unique properties. . Therefore, tremendous efforts have been taken on the synthesis of porous graphene-based materials with unique porous structure providing higher surface area, abundant mass transfer channels, tunable bandgap, high pore edge activity, gas permeability, good mechanical stability and biochemical sensing [18]. To date, different strategies have been successfully developed to prepare porous graphene such as porous graphene nano architectures using silver nanoparticles, activation of exfoliated graphene oxide (GO) with KOH, hydrothermal steam etching of GO nanosheets, controlled catalytic oxidation, laser

irradiation and electron beam irradiation [19–23]. Electrochemical activity of PGNR is further improved by incorporating noble metal nanoparticles into PGNR. Among numerous nanoparticles, AuNPs are considered as an excellent support material due to their remarkable surface chemical properties [24], higher chemical stability, excellent catalytic activity[25], biocompatibility [26] and other notable properties [27–30]. In this work, for the first time a hybrid nanomaterial comprising of porous graphene nanoribbon and AuNPs is fabricated through chemical reduction method. Porous graphene nanoribbon was obtained by etching Fe_2O_3NPs/GNR using hydrochloric acid. AuNPs were electrochemically deposited on PGNR and the obtained AuNPs/PGNR hybrid nanomaterial was applied as a novel immunosensor electrode to detect AFP.

2. Materials and Methods

2.1 Materials

Alpha-fetoprotein antibody and antigen were purchased from Biocell Co. (Zhengzhou, China). Bovine serum albumin (BSA, 96–99%) and multi-walled carbon nanotubes (MWCNT), carbon > 95% 6 - 9 nm O.D x 5 µm L were procured from Sigma (USA). Phosphate buffer solution (PBS), conc. sulphuric acid (H_2SO_4), 88% ACS ortho phosphoric acid (H_3PO_4), iron sulphate ($FeSO_4$), potassium permanganate ($KMnO_4$), 30% hydrogen peroxide (H_2O_2), 35% hydrochloric acid (HCl), 98% hydrazine hydrate $(NH_2)_2$: H_2O, chloroauric acid ($HAuCl_4$) potassium ferrocyanide ($K_4Fe(CN)_6$) and potassium ferricyanide ($K_3Fe(CN)_6$) were purchased from Merck India. All the electrolytes were prepared with ultrapure water (>18 M Ω cm) from a Millipore Milli-Q water purification system.

2.2 Experimental

2.2.1 Synthesis of porous graphene nanoribbon

As illustrated in Figure 1, 300 mg of graphene oxide nanoribbons (GONR) (Figure S1) obtained by unzipping of multiwalled carbon nanotube *via* improved method [31] was mixed with 0.01 M $FeSO_4.7H_2O$ stock solution in which 2.8 g of $FeSO_4.7H_2O$ was dissolved in 1 mL concentrated sulfuric acid. After sonicating for 1 h, iron hydroxide GONR mixture obtained by the following reaction was kept under stirring with 10 mL hydrazine hydrate for 12 h at 80° C in nitrogen atmosphere.

$$FeSO_4.7H_2O + H_2SO_4 \xrightarrow{H_2O} Fe(HSO_4)_2 \xrightarrow{-H_2SO_4} Fe(OH)_2 + H_2O$$

The reduced iron oxide/graphene nanoribbon (Fe_2O_3/GNR) nanocomposite was rinsed with distilled water, acetone and vacuum dried for 24 h at room temperature. Finally, porous

structured GNR was obtained through the removal of iron particles by stirring Fe_2O_3/GNR nanocomposite with 10 mL of 15% concentrated HCl for 6 h. It was further rinsed with distilled water and acetone before vacuum dried at room temperature for 24 h.

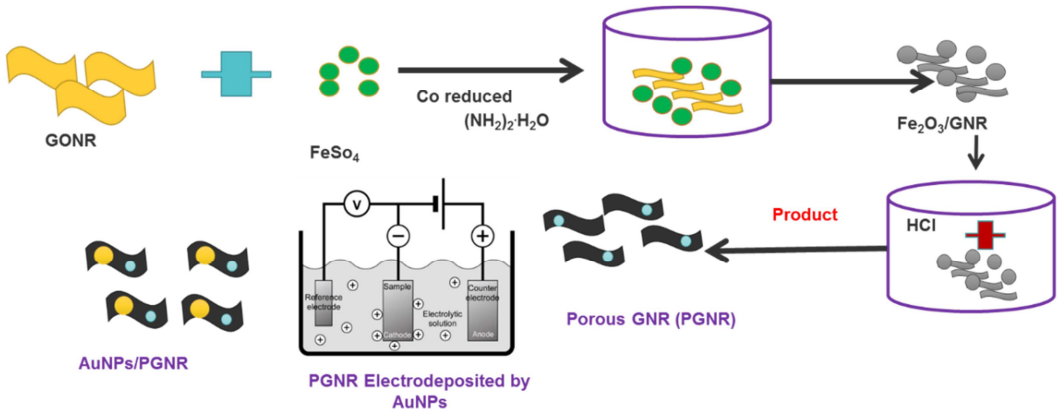

Figure 1. Schematic representation of the synthesis of AuNPs/PGNR.

2.2.2 Electro deposition of AuNPs on PGNR

The AuNPs, an immobilization platform for biomolecules, was electrochemically deposited on PGNR by performing amperometry at a constant potential of -0.2 V for 120 s in 0.5 M H_2SO_4 with 1 g $HAuCl_4$ [29].

2.3 Characterization

The morphology and elemental compostion of the as-synthesized materials were characterised by high resolution scanning electron microscopy (HRSEM) (FEI Quanta FEG 200, HRSEM) and Energy Dispersive X-Ray spectra (EDX) were recorded by JEOL JSM-6700F microscope (Japan).The phase composition of all samples was determined by X-ray diffraction (XRD), PANalytical X-ray diffractometer X'Pert with a Cu Kα radiation (λ = 1.5406 Å). The Brunauer Emmett Teller (BET) surface area was measured by BELSORP-mini II (BEL Japan, Inc.) using N_2 as the adsorption gas. The structural properties of the samples was carried out using Raman spectroscopy WiTech alpha 300 CRF System excited at 532 nm. All Electrochemical measurements were conducted using a potentiostat/ galvanostat PG 302N, AUT 83909 (Metrohm, Autolab, Netherlands) with a conventional three-electrode system in the presence of electrolyte, PBS aqueous solution, of pH 7.4.

2.3 Fabrication of immunosensor

The working electrode of the electrochemical immunosensor was fabricated as follows: GCE polished with 0.3 mm and 0.05 mm gamma alumina particles which was rinsed and sonicated using distilled water, ethanol; and dried under a stream of nitrogen.

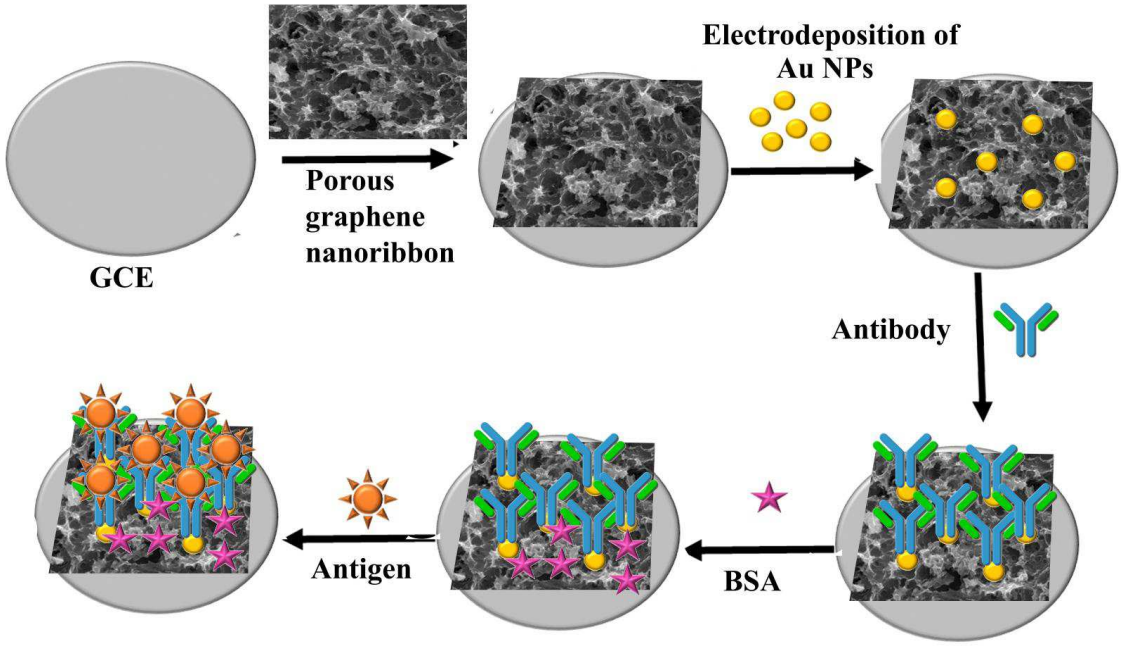

Figure 2. Schematic representation of the AuNPs/PGNR/GCE electrochemical immunosensor for the detection of AFP.

GCE was modified by coating with 7 μL suspension of GONR, GNR and PGNR dispersed separately in DMF (1 mg/ 2 mL) by drop casting method on the electrode surface and was dried at room temperature under vacuum. The stepwise assembly of the proposed immunosensor is illustrated in Figure 2. Firstly, AuNPs were deposited on PGNR modified electrode and then dried in air. Next, 6 μL of anti-AFP (100 μg mL^{-1}) was cast on AuNPs/PGNR/GCE modified electrode surface and incubated for 1h. Subsequently, to avoid interaction between anti-AFP/AuNPs/PGNR/GCE and non-specific adsorbed antigens, the fabricated immunosensor was incubated for 1 h in 4 μL of 0.25% bovine serum albumin (BSA). After rinsing with PBS, the fabricated immunosensor was ready for measurement. The fabricated immunosensor was stored at 4 °C when not in use. The electrochemical signal response was recorded by differential pulse voltammetry (DPV) in the PBS at pH=7.4, in a potential range of 0.2 to 1.2 V.

3 Results and Discussion

3.1 Morphological studies

The morphology and elemental composition of Fe_2O_3/GNR and PGNR observed by HRSEM are illustrated in Figure 3. Figure 3(a) clearly shows that the Fe_2O_3 particles with a size of about 40-50 nm are randomly distributed onto the surface of GNR.

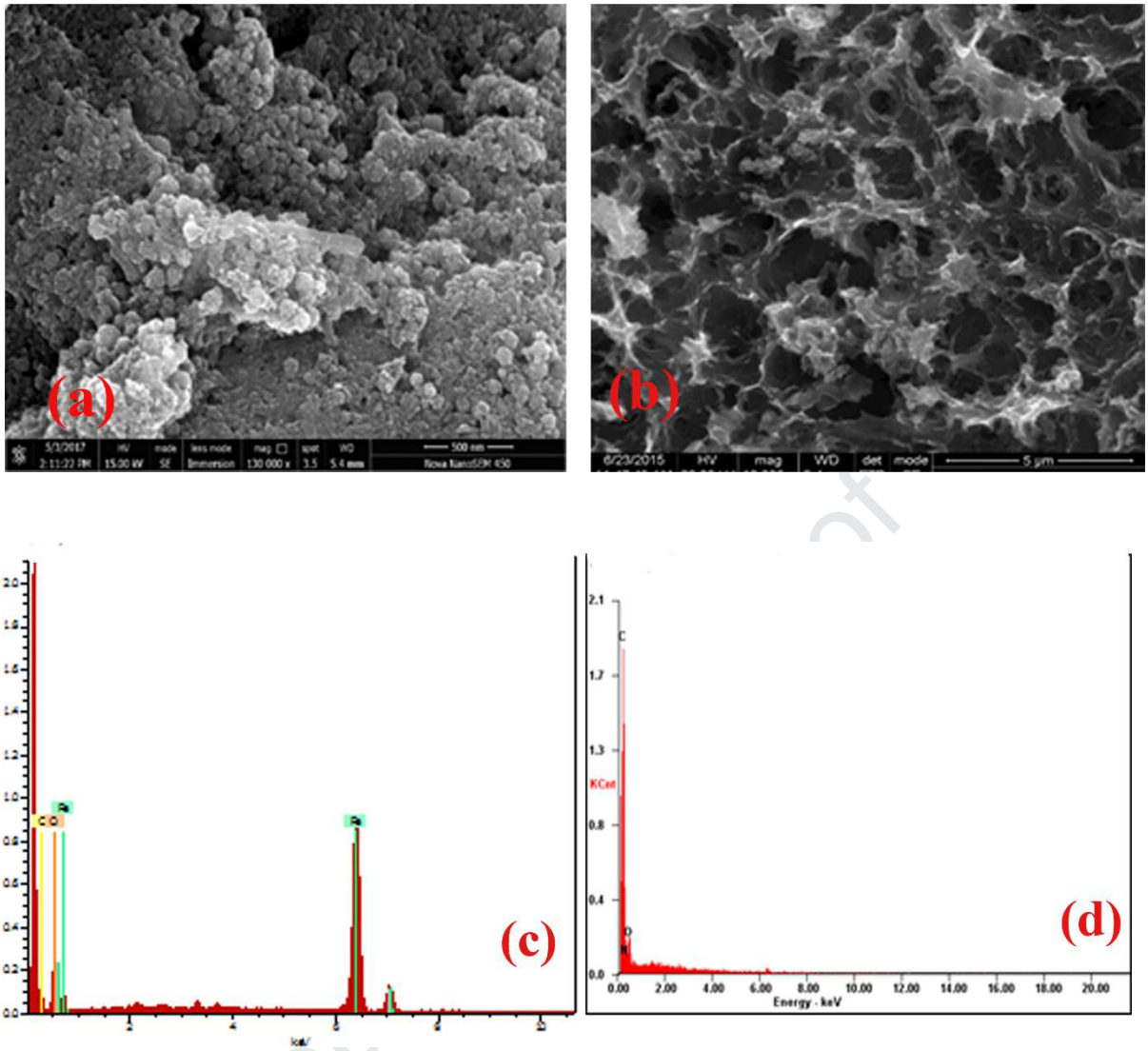

Figure 3 HRSEM images of (a) Fe_2O_3/GNR (b) PGNR with their respective EDX (c & d)

The porous structure, generated upon removal of Fe nanoparticles from Fe_2O_3/GNR was validated from the HRSEM image observed in Figure 3(b)) [32,33]. The porous structured PGNR not only increases the specific surface area, but also prevents agglomeration tendency of graphene nanoribbons. Furthermore, the corresponding energy dispersive X-ray EDX analysis of Fe_2O_3/GNR shown in Figure 3(c), exhibiting strong peaks of C, O and Fe, suggests the formation of a Fe_2O_3/GNR hybrid. Moreover, the EDX measurement of PGNR clearly (Figure 3(d)) evidences the effective removal of Fe particles.

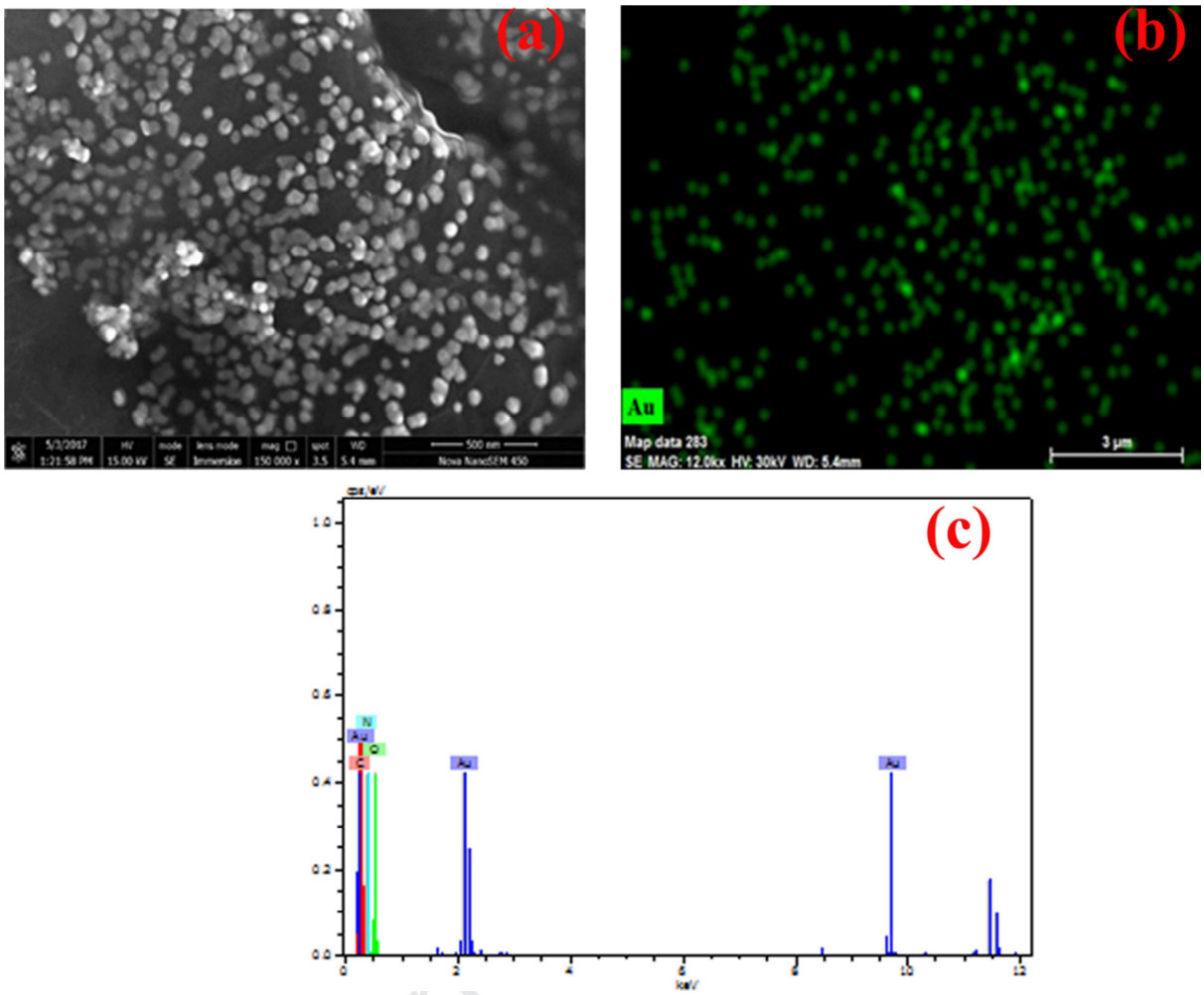

Figure 4 HRSEM image of (a) AuNPs/PGNR its respective elemental mapping and EDX (b & c)

The morphology of AuNPs/PGNR as observed in Figure 4 (a) reveals that spherical shaped AuNPs with a diameter of 30 to 40 nm are homogeneously decorated on the PGNR. Elemental quantification with mapping further illustrates the uniform deposition of AuNPs over PGNR surface in AuNPs/PGNR hybrid (Figure 4(b)). Moreover, EDX analysis of the AuNPs/PGNR hybrid confirms the presence of the Au element along with C in the AuNPs/PGNR hybrid (Figure 4(c)).

3.2 XRD

The crystal structure of GONR, Fe_2O_3/GNR and PGNR were studied by XRD and elucidated in Figure S2. The XRD pattern of GONR is illustrated in Figure S2(a) displays a diffraction peak at 2θ=8°, corresponding to unzipping of MWCNT. The diffraction peaks of obtained Fe_2O_3/GNR hybrid depicted in Figure S2(b) at 2θ of 33.2°, 35.6°, 40.8°, 49.5°, 54.1° and 62.5° corresponding to (104), (110), (113), (024), (116) and (214) crystal planes, respectively reveals the well crystalline nature of hematite phase (JCPDS no. 97-002-2505)

[34,35]. The diffraction peak at around 25° corresponding to (002) plane in PGNR, indicates a successful synthesis of PGNR (Figure S2(c)).

3.3 Raman spectroscopy

The information about the structural properties of modified GONR was acquired from Raman spectroscopy. As shown in Figure S3, the Raman spectra of GONR, Fe_2O_3/GNR and PGNR display two prominent peaks, corresponding to D and G bands. The G band at 1570 cm^{-1} represents the first order scattering of the E_{2g} mode of sp^2 C atoms and the D band at 1336 cm^{-1} is due to the structural imperfection of the A_{1g} mode. From the intensity of G band (I_G) and D band (I_D), the average crystallite size of the sp^2 domains in graphene based materials was measured by the well-known Tuinstra and Koenig (TK) relation.

$$L_a = 4.956\left(\frac{I_G}{I_D}\right)$$

Where, L_a represents the average crystallite size of sp^2 domains and the value 4.956 was obtained from the equation C(λ)= -12.6+0.33 λ. λ indicates the laser wavelength, 532 nm.

The average crystallite size of sp^2 domains in GONR, Fe_2O_3/GNR and PGNR is calculated as 8.26, 5.98 and 4.54 nm, respectively. Reduced average crystallite size in the case of PGNR, compared to Fe_2O_3/GNR and GONR, results in the formation of defects and disorders after modification of GONR [36,37].

Moreover, the ratio between the intensity of D and G band was effectively used to evaluate the degree of disorder in the given samples. I_D/I_G ratio of GONR was increased from 0.6 to 0.92 & 1.09 for Fe_2O_3/GNR hybrid and PGNR respectively. The increased I_D/I_G ratio reveals the increased disorder and defect density generated during the transformation of sp^2 to sp^3 configuration and additional defects introduced in each step of modification.

3.4 Surface area analysis

The nitrogen adsorption/desorption isotherm of the PGNR displays a typical IUPAC type-IV adsorption isotherm pattern with a hysteresis loop, suggests an increase in the specific surface area of PGNR as 132 $m^2 g^{-1}$ by the BET measurement, whereas the specific surface area of reduced graphene oxide (RGO) was only 20 m^2g^{-1}. The increased surface area of PGNR further confirms that the porous structure effectively prevents the restacking property of GNR.

3.5 Optimization of experimental conditions

To achieve better electrochemical performance, it is necessary to optimize the pH and concentration of PGNR, which influence the electron transfer and activity of AFP and anti-AFP. However, acidic or alkaline pH value of buffer would damage the immobilized protein,

the experiment was optimized by PBS at different pH between 5.0 and 8.0. The current responses obtained from CV towards different pH shown in Figure S4 (a) reveals that the peak current increases with increase in pH from 6 to 7.5. After reaching a maximum value at pH 7.5, the peak current decreased with further increase of pH, indicating the optimum pH of 7.5 for this immunosensor. Thus, PBS at physiological pH 7.4 which is closest to 7.5 was used as the electrolyte for electrochemical measurement throughout this study.

In addition, the effect of PGNR concentration on the electrochemical response of the immunosensor was also investigated. As shown in Figure S4(b), with an increase in PGNR concentration from 0.5 to 2 mg/mL, the current response increased, with further increase in concentration, the electroactive sites on the electrode get decreased, resulting in a decrease in the current response. Therefore, optimal concentration of 2 mg/mL PGNR solution was preferred for further experiments in this study.

3.6 Electrochemical characterization of the immunosensor

Cyclic voltammetry (CV) and electrochemical impedance spectroscopy (EIS) depicted in Figure S5 and Figure S6 evidence the stepwise fabrication of immunosensor. Maximum peak current observed in CV of AuNPs/PGNR/GCE (Figure S5, curve a) indicates its enhanced electrocatalytic property. A gradual decrease in peak current observed in anti-AFP/AuNPs/PGNR/GCE (Figure S5, curve b), and BSA/anti-AFP/AuNPs/PGNR/GCE (Figure S5, curve c) indicates the successful immobilization of anti-AFP and BSA on the electrode. Further, a decrease in peak current observed after detection of AFP on BSA/anti-AFP/AuNPs/PGNR/GCE demonstrates the antibody–antigen reaction and successful fabrication of immunosensor (Figure S5, curve d). The decrease in peak current in each step of fabrication is due to the hindrance observed towards the transfer of electrons.

The step wise fabrication of the immunosensor was further characterized by EIS *via* Nyquist plots (Figure S6), which was recorded from 1 to 10^5 Hz in a solution containing 0.1 M PBS (pH 7.4) of $[Fe(CN)_6]^{3-/4-}$.The obtained data of all the modified electrodes were fitted by a Randles equivalence circuit model, including the Warburg impedance (Z_w), the charge transfer resistance (R_{ct}), the double layer capacitance (C_{dl}) and ohmic resistance of the electrolyte (R_s). The EIS includes a semicircle portion and a line. The semicircle portion at higher frequency expresses the electron-transfer limited process, and the corresponding diameter is equal to the R_{ct}. After fitting the data the R_{ct} value of 3200 Ω (curve a) observed in bare GCE implies a low-charge-transfer resistance of the redox couple. PGNR/GCE, AuNPs/PGNR/GCE modified electrodes shows a decrease in R_{ct} to 320 Ω and 175 Ω (curve b and c) respectively, indicating enhanced conductivity of both the modified electrode.

Anti-AFP immobilized on AuNPs/PGNR/GCE, blocks the active sites of the modified electrode and hinders the interfacial electron transfer between the redox probe and the modified electrode, thereby increase the charge transfer resistance to 6600 Ω (curve c). Further increase in R_{ct} to 13000 Ω observed after incubating a non-conductive bioactive substance BSA on anti-AFP/AuNPs/PGNR/GCE indicates the successful immobilization of BSA on the electrode (curve d). Increase in the R_{ct} to 18300 Ω observed after sensing of AFP on BSA/anti-AFP/AuNPs/PGNR/GCE (curve e) demonstrates the effective specific recognition between antibodies and antigens.

3.7 Concentration studies

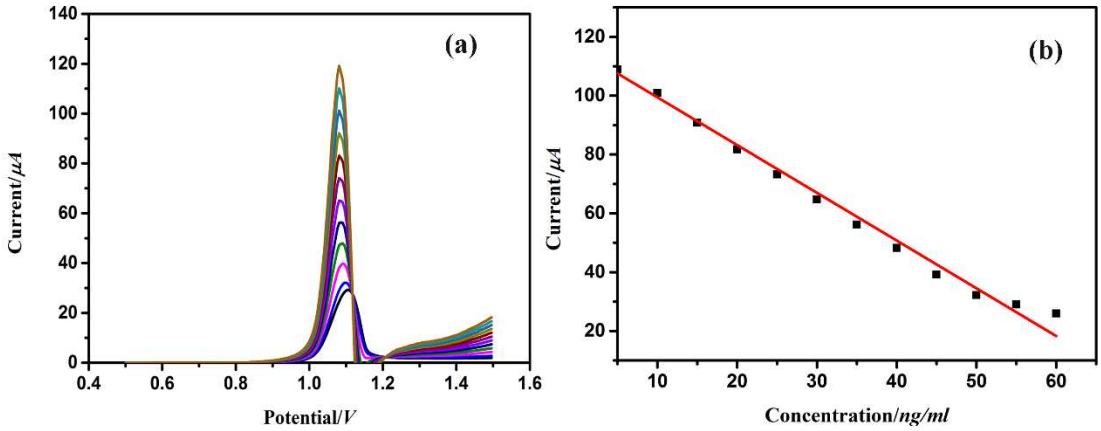

Figure 5 DPV of the fabricated immunosensor at different concentrations of AFP from 5 to 60 ng/mL (a) and the respective calibration curves between peak current and concentration of AFP (b).

Under optimal conditions, the performance of the prepared immunosensor was examined by DPV. The fabricated immunosensor was implemented for the detection of AFP antigen with different concentrations from 5 to 60 ng/ml. Figure 5 (a) showed the electrochemical current responses obtained from DPV towards the addition of AFP antigen for the concentration range of 5 to 60 ng/mL.

The decrease in peak current observed with an increase in AFP concentration as shown in Figure 5(a), indicates the non-conducting antigen AFP bound to the antibody hinders the electron transfer efficiency. The corresponding calibration plots displayed in Figure 5(b) implies a good linear relationship for a concentration range of 5-60 $ng.mL^{-1}$ between electrochemical current responses and the AFP concentration with a correlation coefficient of R^2 =0.99 and a limit of detection of 1 ng/mL.

3.8 Selectivity, stability and repeatability

The immunosensor selectivity could be investigated with 10 ng/mL AFP in the presence of interfering agents, which potentially coexist with AFP in human serum. The interfering agents like UA, DA, AA and glucose were incubated with 10 ng/mL AFP. Negligible change in the current value demonstrated (Figure S7) towards the interfering substances, indicates the high selectivity of as fabricated immunosensor towards AFP. The repeatability of the immunosensor was evaluated (Figure S8), using five electrodes for the detection of AFP (10 ng/mL). Obtained current response elucidates the excellent repeatability of this immunosensor, with relative standard deviation (RSD) less than 5%. The long-term storage stability of immunosensor, stored in PBS (pH 7.4) at 4°C, was also determined by measuring the current response after 30 days. The current response measured every six days as demonstrated in Figure S9, implies a very little decay in the peak currents (barely 5.3%). This clearly shows that proposed immunosensor retains excellent stability over a period of 30 days with 90.6 % current response.

We speculate that the long-term stability and repeatability of the BSA/anti-AFP/AuNPs/PGNR modified immunosensor could be ascribed to three reasons: (1) the BSA/anti-AFP/AuNPs/PGNR film has good stability, (2) the biocompatibility of the AuNPs/PGNR is excellent, and (3) the antibody is tightly attached to the electrode. The better repeatability, high selectivity and good stability confirmed that the as-prepared immunosensor is suitable for quantitative determination of AFP in real human samples. The performance of the PGNR/AuNPs immunosensor was compared with other nanomaterial (Table 1). It can be seen, that the developed immunosensor exhibited comparable linear range and lower detection limit.

Table 1. The performance comparison of the developed immunosensor with other different Au based AFP immunosensor

S.No	Electrode material	Linear range	Limit of detection	Reference
1	Au/AET/PAMAM	5–500 ng/mL	3 ng/mL	[38]
2	Au/PA	5–80 ng/ml	3.7ng/mL	[39]
3	HRP-MPS/PVA/ITO	1-90 ng/mL	0.5 ng/mL	[40]
4	Self–assembled monolayers AuNPs/HRP	15–350 ng/mL	5 ng/mL	[41]
5	PdNi/N-GNRs	0.0001–16 ng/mL	0.03 pg/mL	[42]

6	Pd nanoplates	0.01 to 75.0 ng/mL	4 pg/mL	[43]
7	Pd–rGO	0.01to12 ng/mL.	5 pg/mL	[44]
8	AuNPs/PGNR	5-60 ng/mL	1 ng/mL	This work

3.9 Real sample analysis

The reliability and precision of the immunosensor for real sample analysis are investigated by standard addition method to detect the recoveries of different concentrations of AFP in the human serum sample. The results obtained are tabulated in Table 2. The recovery of the spiked sample ranging between 99.9% and 102 %, validates the applicability of the proposed immunosensor for real sample analysis.

Table 2 Determination of AFP added in human blood serum with the proposed immunosensor.

Sample	**Added (ng/mL)**	**Found (ng/mL)**	**Recovery (%)**
1	1	1.02±0.03	102
2	5	4.98±0.02	100.4
3	10	9.96±0.09	100.4
4	15	14.98±0.19	100.1
5	20	20.02±0.45	99.9

4 Conclusion

A novel electrochemical immunosensor based on AuNPs/PGNR/GCE for the sensitive detection of HCC displayed a wide range of linear response (5-60 ng/ml) and a low detection limit (1 ng/mL). The immobilized anti-AFP molecules exhibited an excellent electrochemical response selective to the AFP in pH 7.4. The fabricated immunosensor exhibited high sensitivity, good repeatability, and long-term stability in quantitative detection of AFP.

Acknowledgement

Authors thank IIST, VRC VSSC, Trivandrum and IIT Madras for XRD, Raman spectroscopy and SEM.

References

[1] J.R. Gillespie, V.N. Uversky, Structure and function of α-fetoprotein: a biophysical overview, Biochim. Biophys. Acta - Protein Struct. Mol. Enzymol. 1480 (2000) 41–56. doi:http://dx.doi.org/10.1016/S0167-4838(00)00104-7.

[2] T.B. Tomasi, Structure and Function of Alpha-Fetoprotein, Annu. Rev. Med. 28 (1977) 453–465. doi:10.1146/annurev.me.28.020177.002321.

[3] T. Morinaga, M. Sakai, T.G. Wegmannt, T. Tamaoki, Primary structures of human a-fetoprotein and its mRNA (cDNA clones/three-domain structure/molecular evolution), Biochemistry. 80 (1983) 4604–4608.

[4] K.J. Alpert, E., Starzl, T. E., Schur, P. H. & Isselbacher, Serum-fetoprotein in hepatoma patients after liver transplantation., Gastroenterology. 61 (1971) 144–148.

[5] I. Štefanová, V. Hořejší, H. Krištofová, P. Angelisová, V. Žižkovský, I. Hilgert, Monoclonal antibodies against human α-fetoprotein exploitation of an unusual calcium-dependent interaction with the antigen for analytical and preparative purposes, J. Immunol. Methods. 111 (1988) 67–73. doi:http://dx.doi.org/10.1016/0022-1759(88)90060-9.

[6] S.K. Sahoo, A. Marikani, Synthesis, characterization and application of electroless metal assisted silicon nanowire arrays, Appl. Surf. Sci. 357 (2015) 1944–1950. doi:10.1016/j.apsusc.2015.09.150.

[7] G. Schnorr, H. Strecker, H.G. Messinger, 367 Specific optimization of a radioimmunoassay for the determination of AFP in oncology, J. Steroid Biochem. 19 (1983) 122. doi:http://dx.doi.org/10.1016/0022-4731(83)91867-8.

[8] C. Zhu, G. Yang, H. Li, D. Du, Y. Lin, Electrochemical Sensors and Biosensors Based on Nanomaterials and Nanostructures, Anal. Chem. 87 (2015) 230–249. doi:10.1021/ac5039863.

[9] Z. Guo, T. Hao, J. Duan, S. Wang, D. Wei, Electrochemiluminescence immunosensor based on graphene–CdS quantum dots–agarose composite for the ultrasensitive detection of alpha fetoprotein, Talanta. 89 (2012) 27–32. doi:http://dx.doi.org/10.1016/j.talanta.2011.11.017.

[10] I.A. Darwish, T.A. Wani, A.M. Alanazi, M.A. Hamidaddin, S. Zargar, Kinetic-exclusion analysis-based immunosensors versus enzyme-linked immunosorbent assays for measurement of cancer markers in biological specimens, Talanta. 111 (2013) 13–

19. doi:http://dx.doi.org/10.1016/j.talanta.2013.03.034.

[11] G.K. Ahirwal, C.K. Mitra, Gold nanoparticles based sandwich electrochemical immunosensor, Biosens. Bioelectron. 25 (2010) 2016–2020. doi:http://dx.doi.org/10.1016/j.bios.2010.01.029.

[12] Q. Gao, J. Han, Z. Ma, Polyamidoamine dendrimers-capped carbon dots/Au nanocrystal nanocomposites and its application for electrochemical immunosensor, Biosens. Bioelectron. 49 (2013) 323–328. doi:http://dx.doi.org/10.1016/j.bios.2013.05.048.

[13] B. Su, D. Tang, Q. Li, J. Tang, G. Chen, Gold–silver–graphene hybrid nanosheets-based sensors for sensitive amperometric immunoassay of alpha-fetoprotein using nanogold-enclosed titania nanoparticles as labels, Anal. Chim. Acta. 692 (2011) 116–124. doi:http://dx.doi.org/10.1016/j.aca.2011.02.061.

[14] H. Hu, M. Feng, H. Zhan, A glucose biosensor based on partially unzipped carbon nanotubes, Talanta. 141 (2015) 66–72. doi:https://doi.org/10.1016/j.talanta.2015.03.057.

[15] Y. Shao, J. Wang, H. Wu, J. Liu, I.A. Aksay, Y. Lin, Graphene Based Electrochemical Sensors and Biosensors: A Review, Electroanalysis. 22 (2010) 1027–1036. doi:10.1002/elan.200900571.

[16] X. Li, X. Wang, L. Zhang, S. Lee, H. Dai, Chemically Derived, Ultrasmooth Graphene Nanoribbon Semiconductors, Science (80-.). 319 (2008) 1229 LP-1232. http://science.sciencemag.org/content/319/5867/1229.abstract.

[17] C. Zheng, X.F. Zhou, H.L. Cao, G.H. Wang, Z.P. Liu, Edge-enriched porous graphene nanoribbons for high energy density supercapacitors, J. Mater. Chem. A. 2 (2014) 7484. doi:10.1039/c4ta00727a.

[18] W. Hooch Antink, Y. Choi, K. Seong, J.M. Kim, Y. Piao, Recent Progress in Porous Graphene and Reduced Graphene Oxide-Based Nanomaterials for Electrochemical Energy Storage Devices, Adv. Mater. Interfaces. 5 (2018) 1701212. doi:10.1002/admi.201701212.

[19] H.-K. Kim, S.-M. Bak, S.W. Lee, M.-S. Kim, B. Park, S.C. Lee, et al., Scalable fabrication of micron-scale graphene nanomeshes for high-performance supercapacitor applications, Energy Environ. Sci. 9 (2016) 1270–1281. doi:10.1039/C5EE03580E.

[20] M.D. Fischbein, M. Drndi, Electron beam nanosculpting of suspended graphene sheets, (2008) 92–94. doi:10.1063/1.2980518.

[21] T.H. Han, Y.-K. Huang, A.T.L. Tan, V.P. Dravid, J. Huang, Steam Etched Porous

Graphene Oxide Network for Chemical Sensing, J. Am. Chem. Soc. 133 (2011) 15264–15267. doi:10.1021/ja205693t.

[22] D. Zhou, Y. Cui, P.-W. Xiao, M.-Y. Jiang, B.-H. Han, A general and scalable synthesis approach to porous graphene., Nat. Commun. 5 (2014) 4716. doi:10.1038/ncomms5716.

[23] Y. Zhu, S. Murali, M.D. Stoller, K.J. Ganesh, W. Cai, P.J. Ferreira, et al., Carbon-Based Supercapacitors Produced by Activation of Graphene, Science (80-.). 332 (2011) 1537 LP-1541. http://science.sciencemag.org/content/332/6037/1537.abstract.

[24] Y.-C. Yeh, B. Creran, V.M. Rotello, Gold nanoparticles: preparation, properties, and applications in bionanotechnology, Nanoscale. 4 (2012) 1871–1880. doi:10.1039/C1NR11188D.

[25] I. Laoufi, M.-C. Saint-Lager, R. Lazzari, J. Jupille, O. Robach, S. Garaudée, et al., Size and Catalytic Activity of Supported Gold Nanoparticles: An in Operando Study during CO Oxidation, J. Phys. Chem. C. 115 (2011) 4673–4679. doi:10.1021/jp1110554.

[26] R. Shukla, V. Bansal, M. Chaudhary, A. Basu, R.R. Bhonde, M. Sastry, Biocompatibility of Gold Nanoparticles and Their Endocytotic Fate Inside the Cellular Compartment: A Microscopic Overview, Langmuir. 21 (2005) 10644–10654. doi:10.1021/la0513712.

[27] Y. Wang, H. Chen, H. Xu, W. Wang, L. Bai, Synthesis of PGMA/AuNPs amplification platform for the facile detection of tumor markers, Mater. Chem. Phys. 183 (2016) 534–541. doi:https://doi.org/10.1016/j.matchemphys.2016.09.012.

[28] P. Sharma, S. Radhakrishnan, S.S. Jayaseelan, B.-S. Kim, Non-enzymatic Electrochemical Oxidation Based on AuNP/PPy/rGO Nanohybrid Modified Glassy Carbon Electrode as a Sensing Platform for Oxalic Acid, Electroanalysis. 28 (2016) 2626–2632. doi:10.1002/elan.201600266.

[29] L. Xiaohui, Electrodeposition of Gold Nanoparticles on Electrochemically Reduced Graphene Oxide for Sensitive Hydrazine Electrochemical Determination in Agriculture Wastewater, Int. J. Electrochem. Sci. 11 (2016) 5279–5288. doi:10.20964/2016.06.94.

[30] J. Wilson, S. Radhakrishnan, C. Sumathi, V. Dharuman, Polypyrrole–polyaniline–Au (PPy–PANi–Au) nano composite films for label-free electrochemical DNA sensing, Sensors Actuators B Chem. 171–172 (2012) 216–222. doi:https://doi.org/10.1016/j.snb.2012.03.019.

[31] D. V Kosynkin, A.L. Higginbotham, A. Sinitskii, J.R. Lomeda, A. Dimiev, B.K. Price,

et al., Longitudinal unzipping of carbon nanotubes to form graphene nanoribbons, Nature. 458 (2009) 872–876.

[32] L.T. Hoa, N. Thi, Y. Linh, J.S. Chung, S.H. Hur, Green synthesis of silver nanoparticle-decorated porous reduced graphene oxide for antibacterial non-enzymatic glucose sensors, Ionics (Kiel). (2017) 0–7. doi:10.1007/s11581-016-1954-0.

[33] H. Zhang, X. Bo, L. Guo, Sensors and Actuators B : Chemical Electrochemical preparation of porous graphene and its electrochemical application in the simultaneous determination of hydroquinone , catechol , and resorcinol, Sensors Actuators B. Chem. 220 (2015) 919–926. doi:10.1016/j.snb.2015.06.035.

[34] R. Wang, C. Xu, J. Sun, L. Gao, J. Jin, C. Lin, Controllable synthesis of nano-LiFePO4 on graphene using Fe2O3 precursor for high performance lithium ion batteries, Mater. Lett. 112 (2013) 207–210. doi:https://doi.org/10.1016/j.matlet.2013.09.037.

[35] T.K.B. Sharmila, J. V Antony, M.P. Jayakrishnan, P.M.S. Beegum, E. Thomas, Mechanical , thermal and dielectric properties of hybrid composites of epoxy and reduced graphene oxide / iron oxide, JMADE. 90 (2016) 66–75. doi:10.1016/j.matdes.2015.10.055.

[36] A. Jorio, Measuring Disorder in Graphene with Raman Spectroscopy, in: E.H.M. Ferreira (Ed.), IntechOpen, Rijeka, 2011: p. Ch. 18. doi:10.5772/15374.

[37] L.M. Malard, M.A. Pimenta, G. Dresselhaus, M.S. Dresselhaus, Raman spectroscopy in graphene, Phys. Rep. 473 (2009) 51–87. doi:http://dx.doi.org/10.1016/j.physrep.2009.02.003.

[38] M. Giannetto, L. Mori, G. Mori, M. Careri, A. Mangia, New amperometric immunosensor with response enhanced by PAMAM-dendrimers linked via self assembled monolayers for determination of alpha-fetoprotein in human serum, Sensors Actuators B Chem. 159 (2011) 185–192. doi:https://doi.org/10.1016/j.snb.2011.06.070.

[39] M. Giannetto, L. Elviri, M. Careri, A. Mangia, G. Mori, A voltammetric immunosensor based on nanobiocomposite materials for the determination of alpha-fetoprotein in serum, Biosens. Bioelectron. 26 (2011) 2232–2236. doi:https://doi.org/10.1016/j.bios.2010.09.040.

[40] J. Lin, Z. Wei, C. Mao, A label-free immunosensor based on modified mesoporous silica for simultaneous determination of tumor markers, Biosens. Bioelectron. 29 (2011) 40–45. doi:https://doi.org/10.1016/j.bios.2011.07.063.

[41] Y.Y. Xu, C. Bian, S. Chen, S. Xia, A microelectronic technology based amperometric immunosensor for α-fetoprotein using mixed self-assembled monolayers and gold nanoparticles, Anal. Chim. Acta. 561 (2006) 48–54. doi:https://doi.org/10.1016/j.aca.2005.12.061.

[42] N. Li, H. Ma, W. Cao, D. Wu, T. Yan, B. Du, et al., Biosensors and Bioelectronics Highly sensitive electrochemical immunosensor for the detection of alpha fetoprotein based on PdNi nanoparticles and N-doped graphene nanoribbons, 74 (2015) 786–791. doi:10.1016/j.bios.2015.07.049.

[43] H. Wang, H. Li, Y. Zhang, Q. Wei, H. Ma, D. Wu, et al., Biosensors and Bioelectronics Label-free immunosensor based on Pd nanoplates for amperometric immunoassay of alpha-fetoprotein, 53 (2014) 305–309. doi:10.1016/j.bios.2013.10.010.

[44] T. Qi, J. Liao, Y. Li, J. Peng, W. Li, B. Chu, et al., Biosensors and Bioelectronics Label-free alpha fetoprotein immunosensor established by the facile synthesis of a palladium – graphene nanocomposite, 61 (2014) 245–250. doi:10.1016/j.bios.2014.05.021.

Highlights

- A novel porous graphene nanoribbon was obtained *via* chemical reduction method
- AuNPs electrodeposited on porous graphene nanoribbon acts as platform for immobilizing biomolecule
- Porous graphene nanoribbon/AuNPs can be used for detection of AFP in human serum.

Author declaration

[Instructions: Please check all applicable boxes and provide additional information as requested.]

1. Conflict of Interest

Potential conflict of interest exists:

We wish to draw the attention of the Editor to the following facts, which may be considered as potential conflicts of interest, and to significant financial contributions to this work:

The nature of potential conflict of interest is described below:

√ No conflict of interest exists.

We wish to confirm that there are no known conflicts of interest associated with this publication and there has been no significant financial support for this work that could have influenced its outcome.

2. Funding

☐Funding was received for this work.

All of the sources of funding for the work described in this publication are acknowledged below:

[List funding sources and their role in study design, data analysis, and result interpretation]

√ No funding was received for this work.

3. Intellectual Property

√ We confirm that we have given due consideration to the protection of intellectual property associated with this work and that there are no impediments to publication, including the timing of publication, with respect to intellectual property. In so doing we confirm that we have followed the regulations of our institutions concerning intellectual property.

4. Research Ethics

☐We further confirm that any aspect of the work covered in this manuscript that has involved human patients has been conducted with the ethical approval of all relevant bodies and that such approvals are acknowledged within the manuscript.

☐IRB approval was obtained (required for studies and series of 3 or more cases)

☐Written consent to publish potentially identifying information, such as details or the case and photographs, was obtained from the patient(s) or their legal guardian(s).

Not applicable

5. Authorship

The International Committee of Medical Journal Editors (ICMJE) recommends that authorship be based on the following four criteria:

1. Substantial contributions to the conception or design of the work; or the acquisition, analysis, or interpretation of data for the work; AND

2. Drafting the work or revising it critically for important intellectual content; AND

3. Final approval of the version to be published; AND

4. Agreement to be accountable for all aspects of the work in ensuring that questions related to the accuracy or integrity of any part of the work are appropriately investigated and resolved.

All those designated as authors should meet all four criteria for authorship, and all who meet the four criteria should be identified as authors. For more information on authorship, please see http://www.icmje.org/recommendations/browse/roles-and-responsibilities/defining-the-role-of-authors-and-contributors.html#two.

√ All listed authors meet the ICMJE criteria. ☐We attest that all authors contributed significantly to the creation of this manuscript, each having fulfilled criteria as established by the ICMJE.

☐One or more listed authors do(es) not meet the ICMJE criteria.

We believe these individuals should be listed as authors because:

[Please elaborate below] ☐

☐We confirm that the manuscript has been read and approved by all named authors.

☐We confirm that the order of authors listed in the manuscript has been approved by all named authors.

6. Contact with the Editorial Office

The Corresponding Author declared on the title page of the manuscript is:

[Insert name below]

Gomathi N

√ This author submitted this manuscript using his/her account in EVISE.

√ We understand that this Corresponding Author is the sole contact for the Editorial process (including EVISE and direct communications with the office). He/she is responsible for communicating with the other authors about progress, submissions of revisions and final approval of proofs.

√ We confirm that the email address shown below is accessible by the Corresponding Author, is the address to which Corresponding Author's EVISE account is linked, and has been configured to accept email from the editorial office of American Journal of Ophthalmology Case Reports:

[Insert email address you wish to use for communication with the journal here]

gomathi@iist.ac.in

☐Someone other than the Corresponding Author declared above submitted this manuscript from his/her account in EVISE:

[Insert name below]

☐We understand that this author is the sole contact for the Editorial process (including EVISE and direct communications with the office). He/she is responsible for communicating with the other authors, including the Corresponding Author, about progress, submissions of revisions and final approval of proofs.

We the undersigned agree with all of the above.

Author's name (Fist, Last)	Signature	Date
On behalf of all authors		
1. __Gomathi Nageswaran_	_____	__6th October 2019_
2. _____	_____	_____
3. _____	_____	_____
4. _____	_____	_____
5. _____	_____	_____
6. _____	_____	_____
7. _____	_____	_____
8. _____	_____	_____
9. _____	_____	_____
10. _____	_____	_____